Electronic Supplementary Information

Composition-Dependent CO_2 Electrochemical Reduction Activity and Selectivity on Au-Pd Core-Shell Nanoparticles

Shangqian Zhu, Xueping Qin, Qi Wang, Tiehuai Li, Ran Tao, Meng Gu,* Minhua Shao*

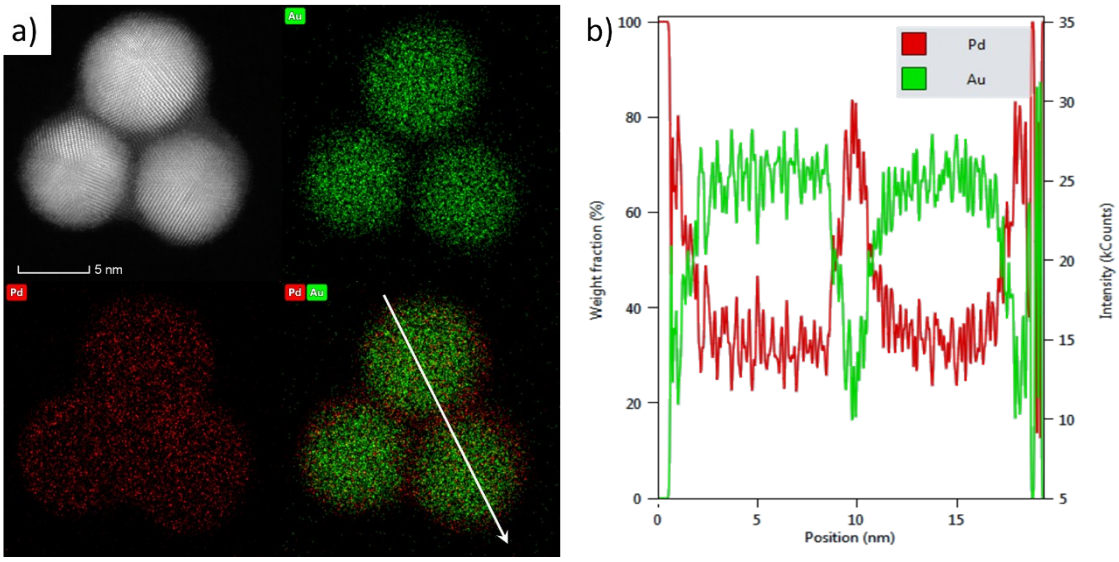

Figure S1. XEDS a) mapping and b) line scan on $Au_{60}Pd_{40}$ nanopartilces.

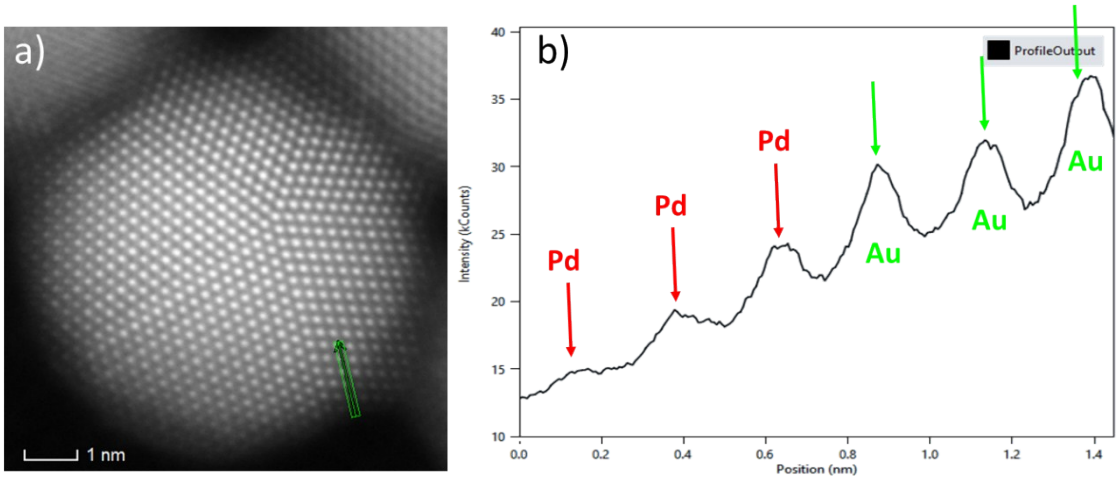

Figure S2. STEM-HAADF a) image and b) intensity profile along the selected scan pathway on $Au_{60}Pd_{40}$ nanoparticles.

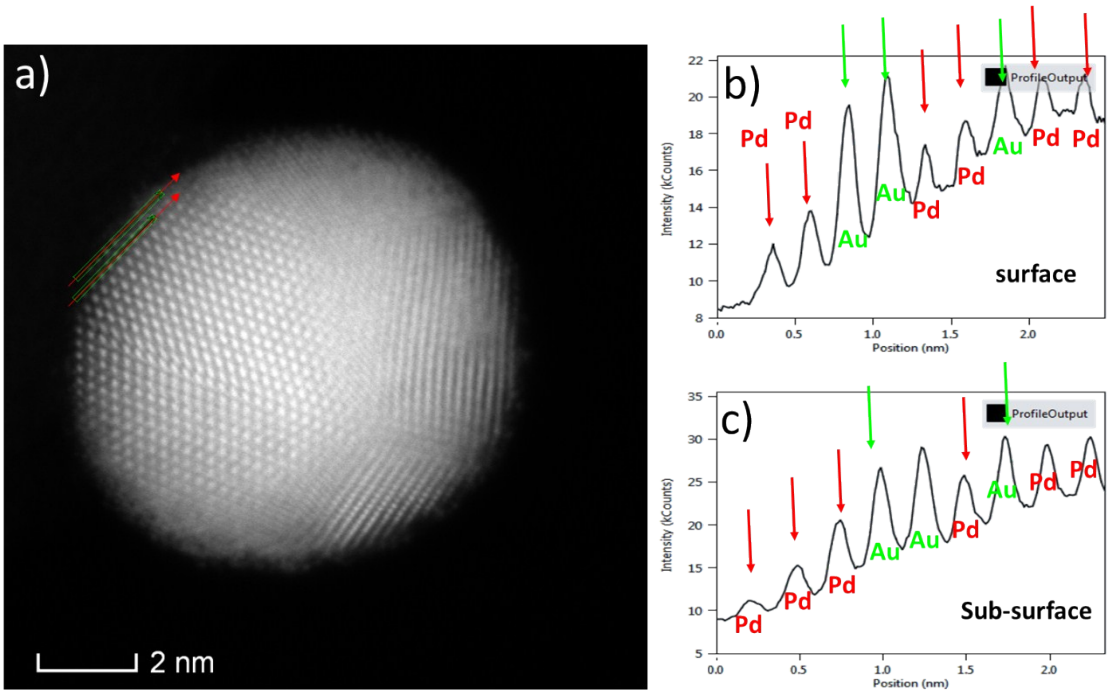

Figure S3. STEM-HAADF a) image and b) intensity profile of the surface and sub-surface layer on $Au_{94}Pd_6$ nanoparticles.

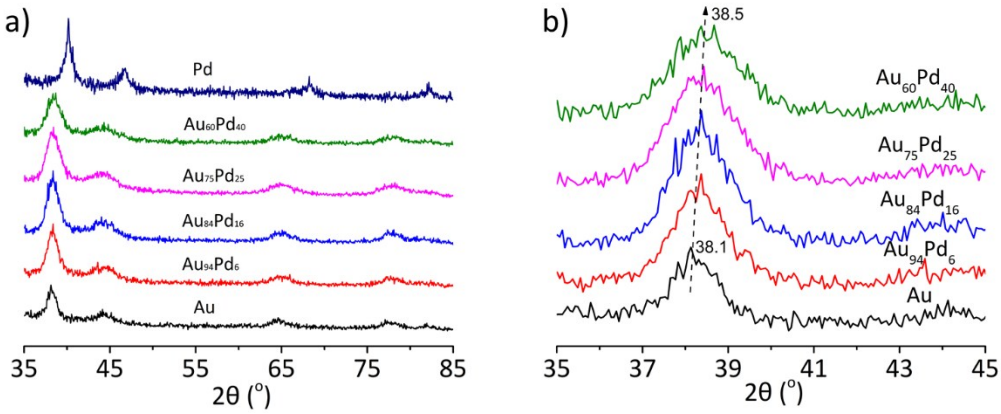

Figure S4. a) XRD patterns of synthesized Au-Pd, Au nanoparticles and Pd/C. b) Enlarged image focused on (111) diffraction peak.

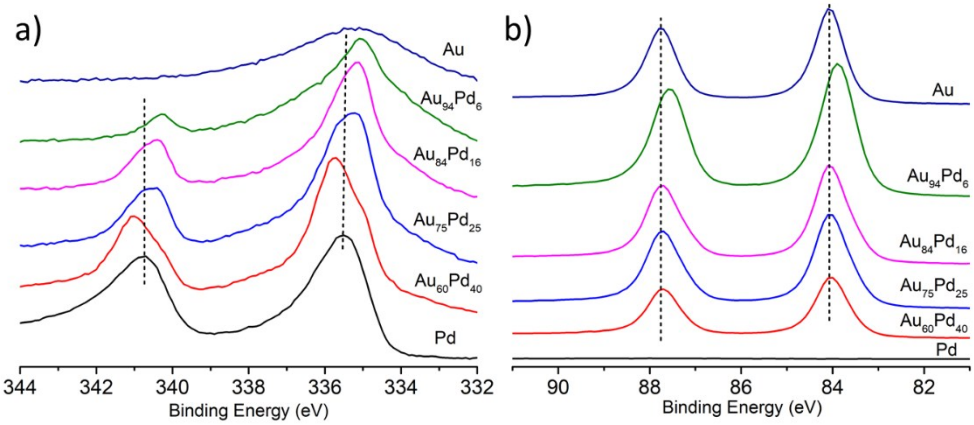

Figure S5. a) Pd 3d and b) Au 4f XPS spectra of synthesized Au-Pd, Au nanoparticles and Pd/C. The binding energy of Pd 3d and Au 4f obtained on pure Pd and Au, respectively, are highlighted with dashed lines for comparison.

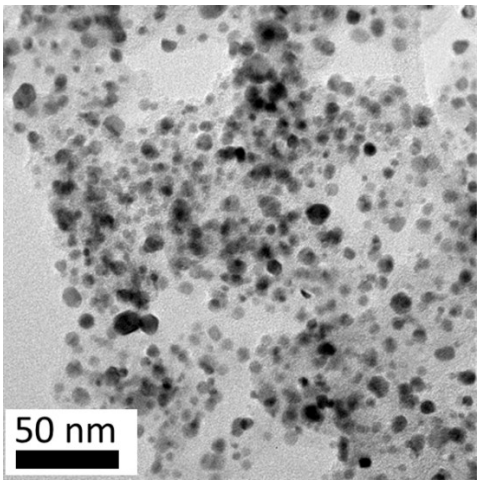

Figure S6. TEM images of Pd/C obtained by sintering commercial Pd/C.

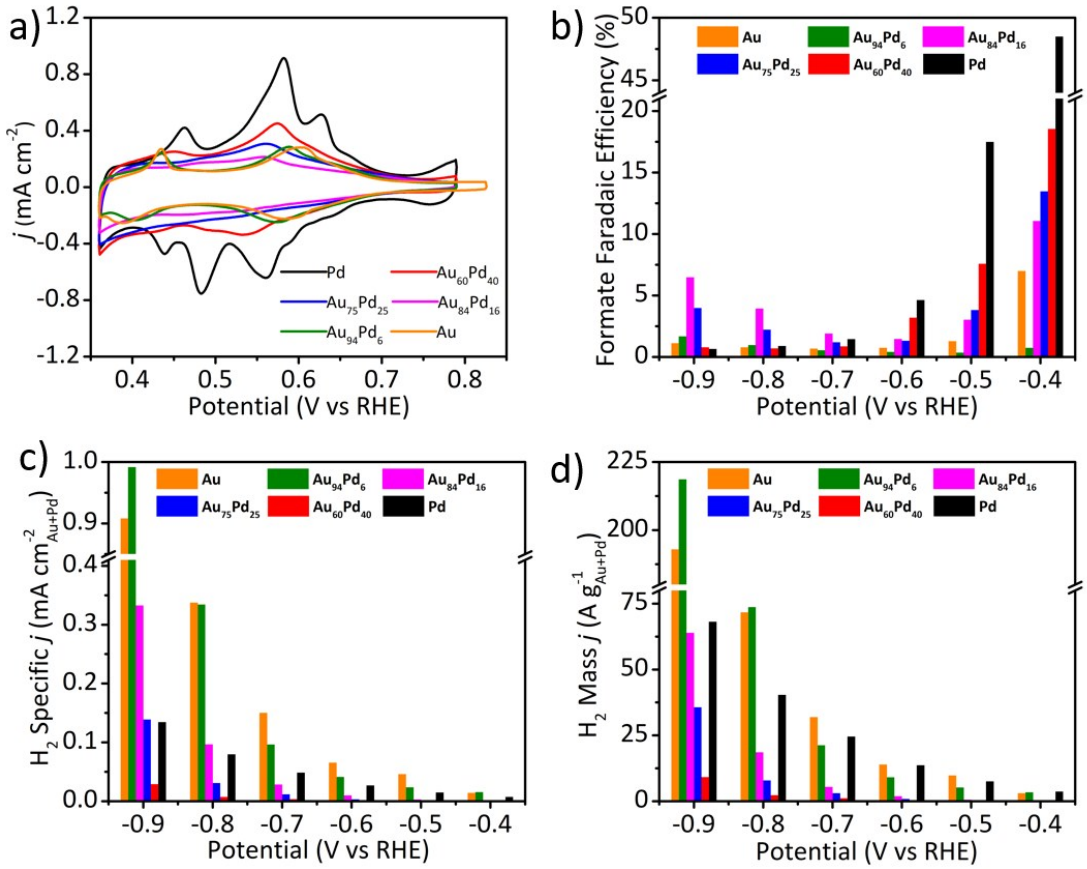

Figure S7. a) Cyclic voltammograms of synthesized Au-Pd, Au nanoparticles and Pd/C in the Ar-saturated 0.05 M $CuSO_4$ + 0.05 M H_2SO_4 solution at a scan rate of 5 mV s^{-1}. b) Faradaic efficiency of formate, c) mass and d) specific activity for H_2 production of synthesized Au-Pd, Au nanoparticles and Pd/C.

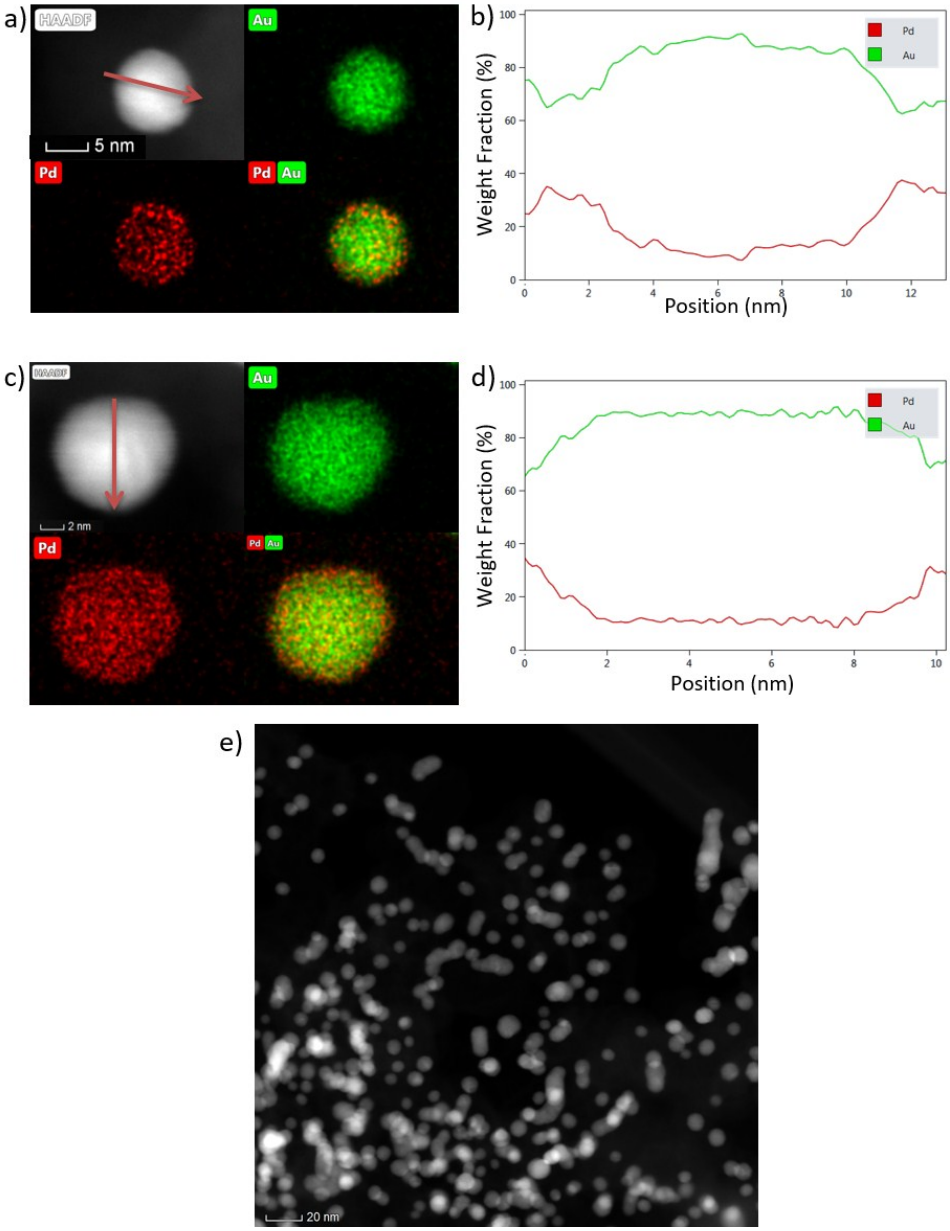

Figure S8. STEM-HAADF images, EDX mapping and line scan profiles of the $Au_{94}Pd_6$ nanoparticles after 12-hour continuous electrolysis at -0.6 V vs RHE.

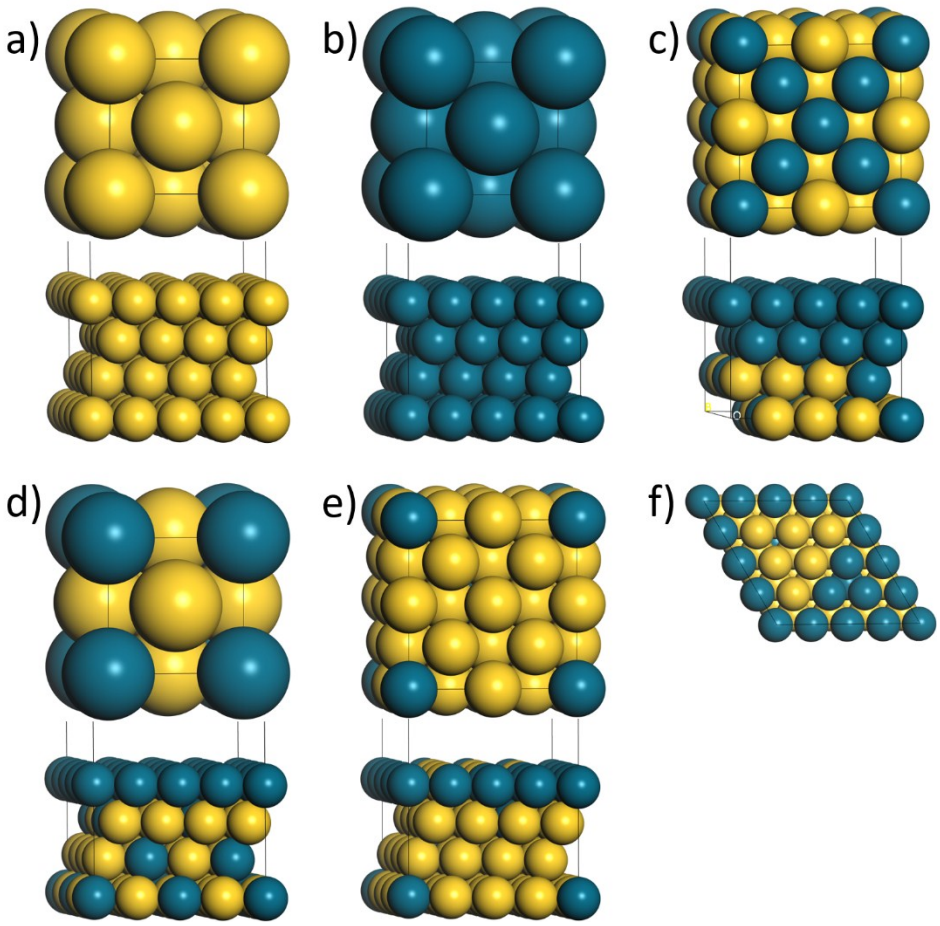

Figure S9. Optimized configurations of catalyst slab models of a) m-Au, b) m-Pd, c) m-$Au_{60}Pd_{40}$, d) m-$Au_{75}Pd_{25}$, and e) m-$Au_{94}Pd_{6}$. The top images are the bulk structure. The bottom images show the structure after the replacement of surface layers. f) The surface element segregation pattern of m-$Au_{94}Pd_{6}$ from the top view. Color code: Pd, blue; Au, yellow.

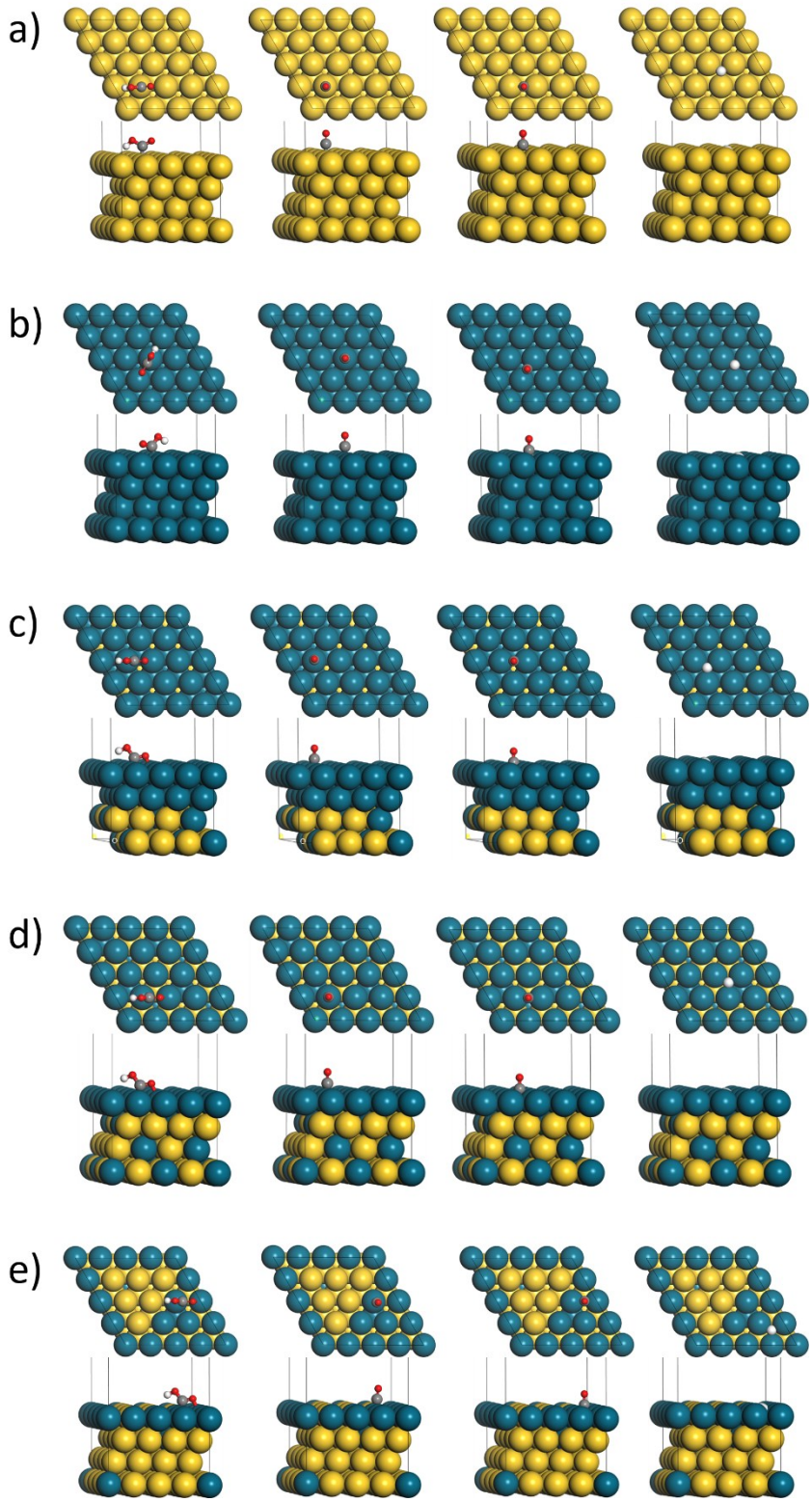

Figure S10. Optimized geometries of *COOH, CO_L, CO_B and *H on a) m-Au, b) m-Pd, c) m-$Au_{60}Pd_{40}$, d) m-$Au_{75}Pd_{25}$, and e) m-$Au_{94}Pd_6$. Color code: Pd, blue; Au, yellow; C, grey; O, red; H, white.

Table S1. Particle size, metal content and specific ECSA of synthesized Au-Pd, Au nanoparticles loaded on carbon black, and Pd/C.

Items	Particle size (nm)	Metal content (%)	Specific ECSA (m^2 g^{-1}_{Pd+Au})
Pd/C	6.1 ± 2.4	33.4	50.7
$Au_{60}Pd_{40}$/C	7.8 ± 2.0	38.4	31.4
$Au_{75}Pd_{25}$/C	7.2 ± 2.0	41.1	25.7
$Au_{84}Pd_{16}$/C	8.1 ± 1.8	42.9	19.2
$Au_{94}Pd_{6}$/C	7.5 ± 1.7	38.7	22.0
Au/C	7.7 ± 1.6	38.5	21.3

Table S2. Overview of catalytic performance of pure Au catalysts

Catalyst	Electrolyte	Maximum FE CO	Mass j_{CO} (A g^{-1}) at ~ -0.5 V	FE CO at ~ -0.5 V
8 nm $Au_{94}Pd_6$ core-shell NP/CB (this work)	**0.5 M $KHCO_3$**	**94.7% (-0.5 V)**	**99.8 (-0.5 V)**	**94.7% (-0.5 V)**
2 nm Au NP/CB[1]	0.5 M $KHCO_3$	~ 65% (-0.8 V)	~3.3 (-0.52 V)	~45% (-0.52 V)
8 nm Au NP/CB[1]	0.5 M $KHCO_3$	90% (-0.67 V)	~2.3 (-0.52 V)	~71% (-0.52 V)
2 nm Au NW/CB[2]	0.5 M $KHCO_3$	94% (-0.35 V)	~5 (-0.5 V)	~90% (-0.5 V)
Grain boundary-rich Au[3]	0.5 M $NaHCO_3$	~96% (-0.55 V)	~14 (-0.5 V)	~95% (-0.5 V)
1.9 nm Au NP on nitrided carbon[4]	0.5 M $NaHCO_3$	~89% (-0.65 V)	~280 (-0.5 V)	~74% (-0.5 V)
Amine-decorated 2.4 nm Au NP[5]	0.1 M $KHCO_3$	~75% (-0.7 V)	~40 (-0.5V)	~30% (-0.5 V)
8 nm Au NP/functional graphene nanoribbon[6]	0.5 M $KHCO_3$	92% (-0.66V)	~23 (-0.57V)	~90% (-0.57 V)

Table S3. Integrated peak area ratio of CO_L and CO_B from ATR-IR spectra collected at different potentials.

at -0.5 V	CO_L (%)	CO_B (%)
Pd/C	3.3	96.7
$Au_{60}Pd_{40}$/C	24.8	75.2
$Au_{75}Pd_{25}$/C	47.4	52.6

at -0.6 V	CO_L (%)	CO_B (%)
Pd/C	3.2	96.8
$Au_{60}Pd_{40}$/C	20.8	79.2
$Au_{75}Pd_{25}$/C	42.4	57.6

at -0.7 V	CO_L (%)	CO_B (%)
Pd/C	3.2	96.8
$Au_{60}Pd_{40}$/C	17.6	82.4
$Au_{75}Pd_{25}$/C	37.5	62.5

Table S4. The DFT calculated energies (E), zero-point energy corrections (ZPE), and entropy corrections (TS) for COOH* and CO* (including CO_L and CO_B) on m-Pd, m-$Au_{60}Pd_{40}$, m-$Au_{75}Pd_{25}$, m-$Au_{94}Pd_6$ and m-Au surfaces. All values are given in eV.

Structures	Adsorbates	E	ZPE	TS	G
m-Pd	COOH*	-342.4309	0.6123	0.2418	0.18
	CO_L	-332.0201	0.1935	0.1873	-0.48
	CO_B	-332.4448	0.1932	0.1374	-0.85
m-$Au_{60}Pd_{40}$	COOH*	-305.7898	0.6201	0.2050	0.08
	CO_L	-295.3665	0.1942	0.1865	-0.60
	CO_B	-295.7945	0.1915	0.1430	-0.99
m-$Au_{75}Pd_{25}$	COOH*	-276.4194	0.6199	0.2064	0.05
	CO_L	-265.9539	0.1954	0.1708	-0.57
	CO_B	-266.4205	0.1907	0.1486	-1.02
m-$Au_{94}Pd_6$	COOH*	-247.0882	0.6192	0.2069	0.19
	CO_L	-236.6656	0.1923	0.1779	-0.49
	CO_B	-237.1107	0.1921	0.1378	-0.89
m-Au	COOH*	-220.9852	0.6067	0.2558	0.98
	CO_L	-210.2060	0.1741	0.2132	0.66
	CO_B	-210.1717	0.1847	0.1459	0.78

Table S5. The DFT calculated energies (E), zero-point energy corrections (ZPE), and entropy corrections (TS) for H* on m-Pd, m-$Au_{60}Pd_{40}$, m-$Au_{75}Pd_{25}$, m-$Au_{94}Pd_6$ and m-Au surfaces. All values are given in eV.

Structures	E	ZPE	TS	G
m-Pd	-319.7616	0.1655	0.0057	-0.43
m-$Au_{60}Pd_{40}$	-283.0341	0.1582	0.0066	-0.49
m-$Au_{75}Pd_{25}$	-253.7163	0.1643	0.0058	-0.56
m-$Au_{94}Pd_6$	-224.4844	0.1618	0.0063	-0.53
m-Au	-198.3124	0.1289	0.0126	0.35

Table S6. The DFT calculated energies (E), zero-point energy corrections (ZPE), and entropy corrections (TS) for small molecules. Gas phase corrections were applied to CO_2 and CO with the value of 0.13 eV and -0.51 eV, respectively.[7] All values are given in eV.

	E	ZPE	TS	Gas phase correction
H_2	-6.72	0.30	0.42	-0.08
H_2O	-14.22	0.59	0.53	-0.06
CO_2	-22.99	0.31	0.62	0.13
CO	-14.80	0.14	0.48	-0.51

References

1 W. Zhu, R. Michalsky, O. n. Metin, H. Lv, S. Guo, C. J. Wright, X. Sun, A. A. Peterson and S. Sun, *J. Am. Chem. Soc.*, 2013, **135**, 16833-16836.

2 W. Zhu, Y.-J. Zhang, H. Zhang, H. Lv, Q. Li, R. Michalsky, A. A. Peterson and S. Sun, *J. Am. Chem. Soc.*, 2014, **136**, 16132-16135.

3 X. Feng, K. Jiang, S. Fan and M. W. Kanan, *J. Am. Chem. Soc.*, 2015, **137**, 4606-4609.

4 L. Jin, B. Liu, P. Wang, H. Yao, L. A. Achola, P. Kerns, A. Lopes, Y. Yang, J. Ho, A. Moewes, Y. Pei and J. He, *Nanoscale*, 2018, **10**, 14678-14686.

5 Y. Zhao, C. Wang, Y. Liu, D. R. MacFarlane and G. G. Wallace, *Adv. Energy Mater.*, 2018, **8**, 1801400.

6 C. Rogers, W. S. Perkins, G. Veber, T. E. Williams, R. R. Cloke and F. R. Fischer, *J. Am. Chem. Soc.*, 2017, **139**, 4052-4061.

7 A. A. Peterson, F. Abild-Pedersen, F. Studt, J. Rossmeisl and J. K. Nørskov, *Energy Environ. Sci.*, 2010, **3**, 1311-1315.